

Simulation of Ultrasound Radio-Frequency Signals in Deformed Tissue for Validation of 2D Motion Estimation with Sub-Sample Accuracy

Orcun Goksel, Reza Zahiri-Azar, and Septimiu E. Salcudean

Department of Electrical and Computer Engineering, University of British Columbia, Vancouver, BC, Canada

Abstract—Motion estimation in sequences of ultrasound echo signals is essential for a wide range of applications. In time domain cross correlation, which is a common motion estimation technique, the displacements are typically not integral multiples of the sampling period. Therefore, to estimate the motion with sub-sample accuracy, 1D and 2D interpolation methods such as parabolic, cosine, and ellipsoid fitting have been introduced in the literature. In this paper, a simulation framework is presented in order to compare the performance of currently available techniques. First, the tissue deformation is modeled using the finite element method (FEM) and then the corresponding pre-/post-deformation radio-frequency (RF) signals are generated using Field II ultrasound simulation software. Using these simulated RF data of deformation, both axial and lateral tissue motion are estimated with sub-sample accuracy. The estimated displacements are then evaluated by comparing them to the known displacements computed by the FEM.

This simulation approach was used to evaluate three different lateral motion estimation techniques employing (i) two separate 1D sub-sampling, (ii) two consecutive 1D sub-sampling, and (iii) 2D joint sub-sampling estimators. The estimation errors during two different tissue compression tests are presented with and without spatial filtering. Results show that RF signal processing methods involving tissue deformation can be evaluated using the proposed simulation technique, which employs accurate models.

I. INTRODUCTION

Estimating the displacements in sequences of ultrasound radio-frequency signal (RF lines) lies at the heart of many signal processing applications including blood flow measurement, tissue velocity imaging, strain rate imaging, and elastography [1], [2], [3]. The most common motion estimation methods are time domain pattern matching techniques, in which the displacements are identified as the maximum/minimum of the pattern matching function between the pre- and post-compression windowed RF lines [4]. Generally, normalized covariance/correlation and sum of squared differences are used as pattern matching functions. The performance of these methods, each offering a trade-off between accuracy, computation complexity, and hardware implementation cost, has been widely studied in the literature [5], [6].

The displacements to be estimated are not necessarily integral multiples of the sampling period. Therefore, the location of the maximum/minimum of the pattern matching function is not an accurate estimator of the actual motion. In order to reduce the bias and variance introduced by the finite sampling intervals, several peak/valley interpolation methods such as curve fitting and polynomial interpolation have been introduced in the literature. The performance of some of

these 1D sub-sampling methods such as parabolic and cosine fitting has been studied in the literature [7], [8].

Although, typically only the axial component of the motion, that is along the beam propagation axis, is estimated, there is also extensive work studying 2D motion estimation [9]. Some 2D motion estimation methods decouple the displacement into two separate axes, where extensions of 1D sub-sampling techniques can be used to estimate both axial and lateral components independently. Alternatively, joint estimation techniques using 2D interpolation methods such as 2D curve fitting and 2D polynomial interpolation can be used to estimate both components simultaneously [10].

The performance of 1D displacement estimators or decoupled 2D displacement estimators can be studied by simulating the deformation of RF signals only in 1D. However, in order to study the performance of joint 2D tracking *with sub-sample accuracy*, a 2D/3D deformation simulation with its corresponding pre-/post-compression simulated RF signals is required. Applying two separate 1D sub-sampling algorithms in order to estimate 2D motion can only be effectively employed in the presence of uncorrelated axial and lateral motion, which is not necessarily the case in actual tissue deformations due to physical constraints.

In this paper, the tissue deformation is modeled using the Finite Element Method (FEM), which was chosen due to its physical validity based on continuum mechanics and its flexibility for expanding to complex elasticity models. The simulated motion is applied to scatterers distributed in 3D in order to find their post-deformation positions. Then, the corresponding pre- and post-deformation RF signals are simulated from these scatterer distributions. Conventionally, this is performed by convolving a point spread function with the distributed scatterers. In this work, we use Field II ultrasound simulation software [11] to simulate RF data with an accurate model of a linear array transducer. 2D tissue motion is then estimated from the sets of simulated RF signals using different tracking algorithms. Their performances are compared by measuring the error between the motion estimated and the motion computed by the FEM.

II. METHODS

Below, the techniques applied for deformation modeling in finding scatterer displacements, simulating RF signals from the distributed scatterers, and estimating tissue motion in RF data are presented.

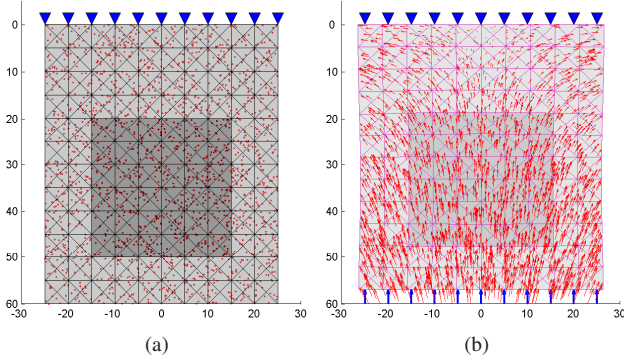


Fig. 1. (a) FEM mesh, deformation constraints, and scatterer distributions (only 2% of all 10^5 scatterers are plotted for better visualization); (b) the displacements of scatterers during tissue compression.

A. Simulation of Deformation and Scatterer Displacements

A 3D virtual phantom is constructed by randomly locating scatterers inside the region of interest. Different scatterer concentrations and amplitudes can be used to adjust spatial echogenicity properties. This virtual phantom is then meshed for FEM deformation simulation. A sample mesh with scatterers inside it can be seen in Fig. 1(a). Post-deformed scatterer positions are interpolated using shape functions in the mesh, the deformation of which is computed using the FEM. Their displacements for a sample compression of 5% of the phantom height are demonstrated in Fig. 1(b).

In the simulations, the ultrasound probe is assumed to be compressing from the top side of the mesh. Nevertheless, images are typically processed in the probe's frame of reference. Thus, in the mesh, the compression is modeled by fixing the top side, touching the probe surface, and moving the bottom side upwards. The displacements of both top and bottom sides are constrained vertically, but not horizontally. This is done considering that the lubricated tissue surface in reality is free to slide on the probe. For a symmetric simulation, the same assumption is applied to both ends. Note that throughout this paper the vertical and horizontal axes here are referred to as the axial and lateral directions, respectively, considering the probe's frame of reference.

B. Simulation of RF data

Various RF simulation techniques have been used in the literature. For instance, the convolution of a pre-computed point-spread function along the scatterers of the phantom is a common method. In our simulations, we use Field II software due to its accurate modeling of transducer properties, beam focusing, wave propagation and interactions [11].

C. Displacement Estimation

In motion estimation, each line in the pre-compression RF signal is commonly divided into overlapping windows. The displacement of each window is then estimated by searching for that window in the post-compression RF signal. Time Domain Cross Correlation with Prior Estimates (TDPE) [12] with normalized correlation as a similarity measure was used

as the motion tracking algorithm. TDPE is a modified version of the standard cross correlation technique. It predicts the motion based on the previously estimated data and monitors the correlation coefficient for validation of the estimated values. A recovery search is triggered when the correlation coefficient drops below a certain threshold (i.e., ≤ 0.9).

Since the deformation is small ($\leq 1\%$) and the lateral motion is less than a full RF-line width, the estimation of the lateral component of the motion is postponed until after the estimation of the axial component of the motion, similarly to [13]. In other words, the lateral motion is ignored during the estimation of the axial motion but is estimated afterwards.

Once a coarse location of the cross correlation function peak is found, three different sub-sampling methods are used to estimate the sub-sample component of the axial and lateral displacements. The first method (i) uses two separate 1D sub-sampling [8]. The second method (ii) uses 1D sub-sampling in the axial direction followed by a second 1D sub-sampling which uses the result from the axial sub-sampling to estimate the lateral sub-sampling [13]. The last method (iii) uses a 2D joint axial/lateral sub-sampling estimator [10].

III. RESULTS

For our experiments, a $50 \times 60 \times 10$ mm virtual phantom was constructed by randomly locating 10^5 scatterers inside it. The deformation of this phantom was modeled using 2D linear FEM with triangular elements. A symmetrical mesh similar to Fig. 1(a) was used with four times finer resolution than shown in this figure. Our mesh has 1005 nodes and 1920 triangles and contains a square inclusion of 30 mm with its Young's modulus being twice that of the substrate. The Poisson's ratio was set to 0.49 for all elements. The average density and amplitude of scatterers were kept the same within and outside the inclusion in order to render it undetectable in the RF signal and B-mode without applying deformation.

In Field II, a linear probe with 5 MHz center frequency and 60 MHz sampling rate was modeled. In this setting, one simulated RF line contains 4600 samples for our phantom depth. 128 RF lines were simulated along a width of 40 mm by 64 transducers firing at a time focusing to a depth of 25 mm. For displacement estimation, RF data were axially broken into 115 overlapping blocks of each 1 mm length and with 50% overlap. This yields $(115 \times 128 =)$ 14720 windows that were used for motion estimation. Fig. 2(a) shows the centers of a small number of such windows (less than 4%). The expected displacements of these locations were also computed using the FEM model as seen in Fig. 2(b) in order to use the results as the *true* motion for assessing the estimation techniques.

Compressions of 0.5% and 1% of the depth were applied to the phantom, resulting in 0.3 and 0.6 mm surface displacements, respectively. The displacements, which are interpolated using an overlaid 2D FEM model, are then applied to the axial and lateral nominal scatterer positions to find their post-deformation positions. Consequently, three sets of RF data were generated: *A*) pre-compression, *B*) 0.5% compression, and *C*) 1% compression. The displacements

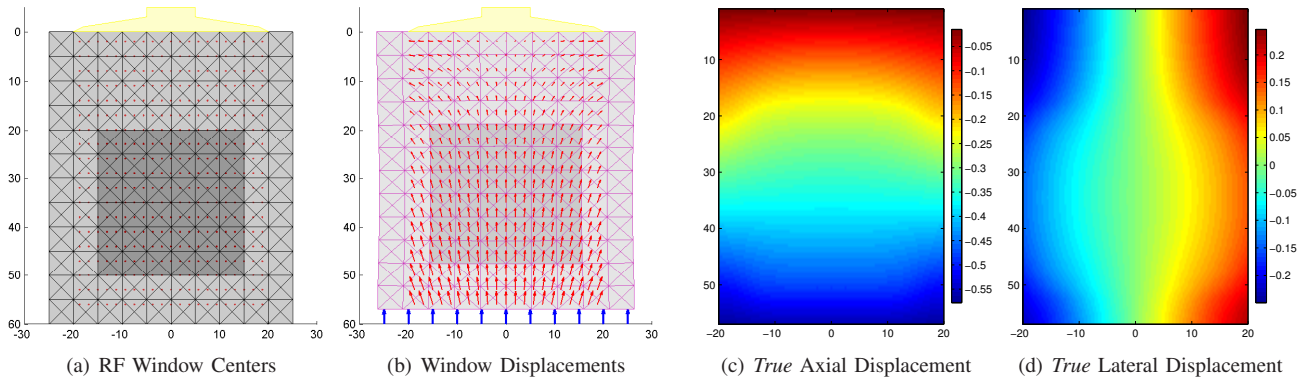


Fig. 2. Centers of RF windows used in motion estimation located in the mesh (a); *true* displacements of these windows computed by the FEM (b) for a sample 5% compression; *true* axial (c) and lateral (d) displacement components for 0.5% compression.

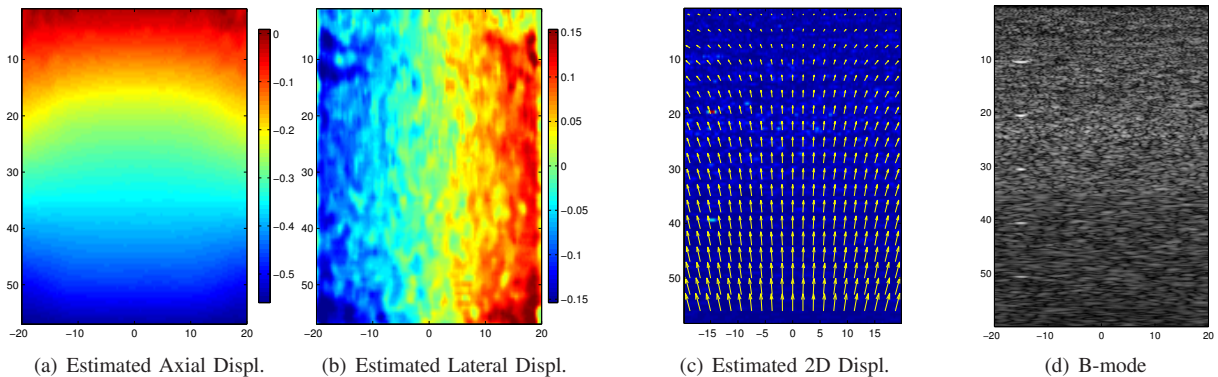


Fig. 3. Estimated axial (a) and lateral (b) displacements using method B; 2D estimated displacement vectors (c); and a simulated B-mode image (d)

were estimated at 14720 window centers from \mathcal{A} to \mathcal{B} and from \mathcal{A} to \mathcal{C} on these simulated RF data. These estimations were then compared with the displacements interpolated at the same locations in the FEM deformation model.

Displacements were estimated using the techniques described in Section II-C. *True* axial and lateral displacements computed by the FEM at given RF window centers are presented for 0.5% compression in Fig. 2(c-d). For the same compression test, the estimated axial and lateral displacements with sub-sample accuracy using technique (ii) can also be seen in Fig. 3(a-b). This 2D estimated motion is shown as a vector field in Fig. 3(c).

The error is found as the difference of each estimated displacement and its *true* FEM interpolated counter-part. For example, Fig. 4(a) shows the axial estimation error for 1% compression. The lateral error of sub-sampling method (ii) is presented in Fig. 4(b). Furthermore, the effect of different filtering kernel sizes on lateral estimation techniques was also studied. For example, the same lateral displacement data is shown in Fig. 4(c-e) after median and Gaussian filtering by 3×3 , 5×5 , and 15×15 kernels.

The mean magnitudes of displacement errors are tabulated in Table I. Since lateral estimation is generally more difficult and less robust, the errors in that axis were compared for the three different approaches. The error values depend on compression magnitude and phantom dimensions, thus they are

also tabulated in Table II after normalizing to the maximum *true* displacement for the corresponding axis/compression.

IV. DISCUSSION

For deformation, other element geometries and/or elasticity models can also be used. Furthermore, a 3D FEM model can be employed in order to allow for simulating possible scatterer motion in the probe's elevational axis and its effect on the motion estimation techniques.

The lateral strips of relatively high errors at the depths of 15, 25, 35 mm (see Fig. 4(a)) are caused by the fixed receive focusing centered at 10, 20, 30, 40, ... mm set in the Field II simulation parameters. Dynamic focusing and other simulation options can be used in order to cope with such artifacts. A sample B-mode image obtained by further processing our simulated RF data is shown in Fig. 3(d).

V. CONCLUSIONS AND FUTURE WORK

As seen in Table I and II, the displacement estimation in the axial direction is on the average an order of magnitude more accurate than the estimations in the lateral direction. This expected result is due to the fact that the ultrasound resolution is much finer in the axial direction. The results also show that estimating the lateral motion with sub-sample accuracy using separate 1D sub-sampling method (i) gives the least accurate results for the compression test applied.

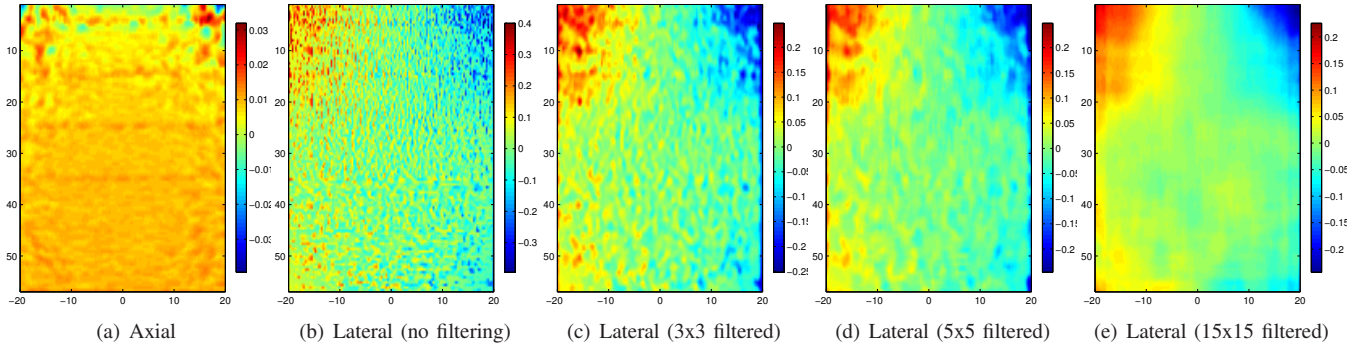


Fig. 4. Axial error (a), lateral error (b) without filtering, and lateral error (c-e) using method (ii) filtered by 3×3 , 5×5 , and 15×15 kernels.

TABLE I

MEAN AND STANDARD DEVIATIONS OF MOTION ESTIMATION ERROR MAGNITUDES IN AXIAL DIRECTION, AND LATERAL DIRECTION USING THREE DIFFERENT SUB-SAMPLING TECHNIQUES FOR TWO COMPRESSION TESTS. THE EFFECT FILTERING IS ALSO PRESENTED.

Motion Estimation Error [mm]	0.5% compression						1% compression					
	No filter		3x3		5x5		No filter		3x3		5x5	
	Mean	Std	Mean	Std	Mean	Std	Mean	Std	Mean	Std	Mean	Std
Axial	0.0087	0.0372	0.0066	0.0218	0.0042	0.0019	0.0261	0.1501	0.0143	0.0445	0.0088	0.0040
Lateral using (i)	0.0677	0.1915	0.0319	0.0413	0.0258	0.0337	0.1017	0.0467	0.0410	1.1967	0.0653	0.0595
Lateral using (ii)	0.0516	0.0649	0.0254	0.0333	0.0215	0.0295	0.0670	0.0899	0.0434	0.0614	0.0392	0.0571
Lateral using (iii)	0.1475	3.4738	0.0264	0.0346	0.0199	0.0275	0.2082	5.3100	0.0401	0.0593	0.0326	0.0519

TABLE II

MOTION ESTIMATION ERROR IN PERCENTAGES NORMALIZED TO THE MAXIMUM ACTUAL DISPLACEMENT IN THE CORRESPONDING AXIS FOR THE GIVEN COMPRESSION TEST. THE EFFECT OF FILTERING ON DIFFERENT ESTIMATION TECHNIQUES IS ALSO PRESENTED.

Motion Estimation Error [%]	0.5% compression						1% compression					
	No filter		3x3		5x5		No filter		3x3		5x5	
	Mean	Std	Mean	Std	Mean	Std	Mean	Std	Mean	Std	Mean	Std
Axial	2.988	12.776	2.267	7.487	1.442	0.653	4.482	25.775	2.456	7.641	1.511	0.687
Lateral using (i)	53.444	151.18	25.183	32.603	20.367	26.604	40.142	472.35	18.433	25.775	16.183	23.485
Lateral using (ii)	40.735	51.234	20.051	26.288	16.973	23.288	26.446	35.485	17.131	24.235	15.473	22.538
Lateral using (iii)	116.44	2742.3	20.841	27.314	15.710	21.709	82.179	2095.9	15.828	23.407	12.868	20.486

This is because axial and lateral motions are correlated in tissue deformation and joint estimation generally performs better in estimating correlated 2D motions.

The techniques presented in this paper were found suitable to accurately simulate ultrasound RF data in response to tissue compression. The presented simulation technique for the validation of motion estimation is also applicable for the assessment of other ultrasound signal processing applications such as static/dynamic elastography. Other motion estimation techniques will next be studied using this simulation approach. It will also be employed for validation of different techniques used for estimating tissue mechanical properties in the future.

REFERENCES

- [1] I. Hein, V. Suorsa, J. Zachary, R. Fish, J. Chen, W. Jenkins, and W. O'Brien, "Accurate and precise measurement of blood flow using ultrasound time domain correlation," in *IEEE Ultrasonics Symp*, vol. 2, Montreal, QC, Canada, Oct 1989, pp. 881–886.
- [2] A. Heimdal, A. Stoylen, H. Torp, and T. Skjaerpe, "Real-time strain rate imaging of the left ventricle by ultrasound," *J Am Soc Echocardi*, vol. 11, pp. 1013–1019, 1998.
- [3] L. Bohs, B. Friemel, and G. Trahey, "Experimental velocity profiles and volumetric flow via two-dimensional speckle tracking," *Ultrasound in Medicine and Biology*, vol. 21, pp. 885–898, 1995.
- [4] J. Ophir, I. Cespedes, H. Ponnekanti, Y. Yazdi, and X. Li, "Elastography: a quantitative method for imaging the elasticity of biological tissues," *Ultrasonic Imaging*, vol. 13, pp. 111–134, 1991.
- [5] F. Viola and W. Walker, "A comparison of the performance of time-delay estimators in medical ultrasound," *IEEE Trans Ultrason Ferroelectr Freq Control*, vol. 50, pp. 392–401, 2003.
- [6] G. Jacovitti and G. Scarano, "Discrete time techniques for time delay estimation," *IEEE Trans Signal Process*, vol. 41, pp. 525–533, 1993.
- [7] I. Cespedes, Y. Huang, J. Ophir, and S. Spratt, "Methods for the estimation of subsample time-delays of digitized echo signals," *Ultrasonic Imaging*, vol. 17, pp. 142–171, 1995.
- [8] F. Viola and W. Walker, "A spline-based algorithm for continuous time-delay estimation using sampled data," *IEEE Trans Ultrason Ferroelectr Freq Control*, vol. 52, pp. 80–93, 2005.
- [9] E. Konofagou and J. Ophir, "A new elastographic method for estimation and imaging of lateral displacements, lateral strains, corrected axial strains and poisson's ratios in tissues," *Ultrasound in Medicine and Biology*, vol. 24, pp. 1183–1199, 1998.
- [10] G. Giunta, "Fine estimators of two-dimensional parameters and application to spatial shift estimation," *IEEE Trans Signal Process*, vol. 47, pp. 3201–3207, 1999.
- [11] J. A. Jensen, "A model for the propagation and scattering of ultrasound in tissue," *J Acoustical Soc Am*, vol. 89, pp. 182–191, 1991.
- [12] R. Zahir-Azar and S. E. Salcudean, "Motion estimation in ultrasound images using time domain cross correlation with prior estimates," *IEEE Trans Biomed Imag*, vol. 53, no. 10, pp. 1990–2000, 2006.
- [13] —, "Real-time estimation of lateral motion using time domain cross correlation with prior estimates," in *IEEE Ultrasonics Symp*, Vancouver, BC, Canada, Oct 2006, pp. 1209–1212.